FLUX-BASED 3D SEGMENTATION OF KERATIN INTERMEDIATE FILAMENTS IN CONFOCAL LASER SCANNING MICROSCOPY

*Gerlind Herberich, Andreas Friedrich, Til Aach**

Institute of Imaging & Computer Vision
RWTH Aachen University
52056 Aachen, Germany

*Reinhard Windoffer**, *Rudolf E. Leube**

Institute of Molecular & Cellular Anatomy
RWTH Aachen University
52056 Aachen, Germany

ABSTRACT

We propose an optimally oriented flux-based method for the 3D segmentation of keratin intermediate filaments (KFs) in images acquired using fluorescence confocal laser scanning microscopy (CLSM). KFs are elastic cables forming a complex scaffolding within epithelial cells that is involved in many basic cell functions. Segmentation of KFs to generate a graph representation of the KF network therefore is a key component for analyzing the KFs' dynamic and biomechanical properties. Our segmentation method follows the principle of line enhancement, thresholding and centerline extraction to yield a one-voxel-wide centerline as result. The method is quantitatively evaluated using synthetic data generated by simulating the imaging process in CLSM. It is compared to segmentation results achieved with well-known vesselness measures. The results show that despite limited image quality in CLSM a high degree of precision is achieved.

Index Terms— Segmentation, Flux, Cytoskeleton, Confocal Laser Scanning Microscopy, Fluorescence Microscopy

1. INTRODUCTION

4D (3D+time) live cell fluorescence imaging by confocal laser scanning microscopy (CLSM) has become a widely used tool in cell biology for the analysis of the dynamics of subcellular structures. In the work presented here, we investigate the properties of keratin intermediate filaments (KFs). They are flexible, filamentous structures of about 10 nm diameter forming a complex scaffolding within epithelial cells (Fig. 1). As part of the cytoskeleton, they are responsible for the mechanical stability of epithelial cells and tissues and are involved in the regulation of many basic cell functions [1, 2].

The network topology is a key component for the analysis of dynamic KF behavior under different conditions. We have acquired 3D images of fluorescently-labeled KF networks by means of CLSM. In CLSM, the three-dimensional specimen is scanned slice by slice, each slice being scanned point-wise. The resulting image is a 3D stack of 2D slices. Due to the anisotropic PSF of a CLSM, the spatial resolution of the 3D image is highly limited in the dimension along the optical axis. Furthermore, the images are strongly corrupted by signal-dependent Photon-counting noise.

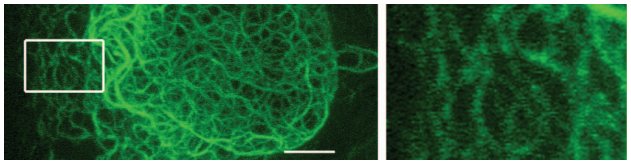


Fig. 1. Left: Maximum-Intensity-Projection of the 3D scaffolding of fluorescently-labeled KFs of a cultured epithelial cell acquired by CLSM. The KFs appear as green bended curves in the image. Bar $5\mu m$. Right: Zoom of boxed area.

In the past, considerable effort has been invested in the 3D segmentation of structures at the supracellular level, which can be imaged with a high spatial resolution in all three dimensions. Concerning bended elongated structures, numerous vessel segmentation approaches have been proposed. To assess whether these approaches are suitable for the 3D segmentation of subcellular filamentous structures whose diameter is close to or below the resolution limit using CLSM images, we have compared some of the most commonly-used approaches [3] showing promising results.

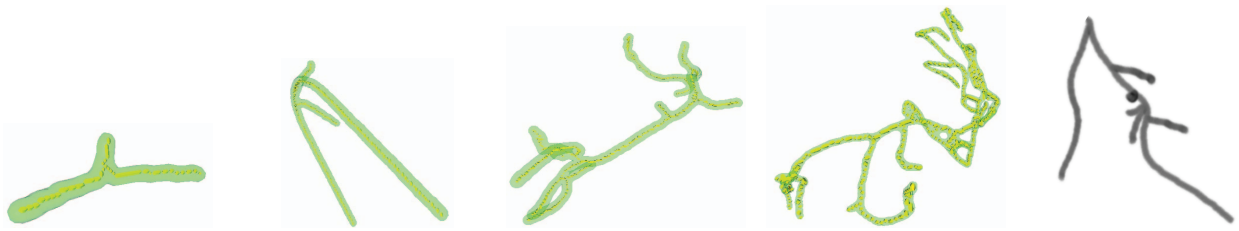
In the recent past, flux driven segmentation approaches have achieved increasing interest. The advantage of flux is its ability to separate closely located parallel lines and its comparatively much less decreasing filter response at branchings which makes flux an interesting feature for the segmentation of KF networks. Here, we present a novel flux-based segmentation method for KF networks.

2. METHODS

2.1. Optimally Oriented Flux for Enhancement Filtering

Many line enhancement filters use the Hessian of Gaussian (e.g. [4, 5, 6]). Hence, they compute the weighted intensity difference between points inside the line and points in the

*The authors gratefully acknowledge funding by the German Research Council (DFG, AA5/5-1, LE566/18-1, WI1731/8-1).



(a) Data set 1 (b) Data set 2 (c) Data set 3 (d) Data set 4 (e) Data sets 5-10

Fig. 2. Synthetic data. Data set 1-4: Volume data as surface representation (green) and ground truth centerline (yellow). Synthetic vessel branchings with 82 centerline points (a) and 303 centerline points (b), and centerlines from real artery geometries with 497 centerline points (c) and 623 centerline points (d). Geometry for data sets 5-10 (e): Synthetic branching tubes (667 centerline points) for the generation of 6 data sets with increasingly anisotropic spatial sampling.

vicinity of the line. Closely located structures thus contribute to the feature computation leading to a poor performance of these filters in case of adjacent structures and branchings. Flux-based measures, instead, evaluate the gradient flux through the boundary of a local sphere. If the surface of the local sphere is aligned with the boundary of an object in the image, the inward flux through the surface is maximal. Consequently, the flux measure becomes maximal at the center of a line with a radius corresponding to the radius of the sphere. Therefore, they avoid including adjacent structures. In [7], optimally oriented flux (OOF) has been proposed as an efficient flux-driven method for line enhancement filtering that has the same complexity as Hessian-based line filtering.

2.2. Centerline Extraction

Our goal is the extraction of a one-voxel wide centerline from the enhanced lines while preserving the connectivity of the network. To this end, we first threshold the line strength image to obtain a binary volume segmentation and then extract the centerline from the binary volume.

The only requirement for the threshold is the preservation of network connectivity, i.e. a false negative rate practically equal to zero. Therefore, a rough conservative estimate of the minimum value of the object class using 2628 object class samples from 6 different synthetic training data sets provides us with a suitable threshold.

Concerning the subsequent centerline extraction, we compare two approaches: The topology-preserving thinning [8, 9] and the more recently proposed flux-based centerline extraction [10, 11]. The method proposed in [8] iteratively thins the binary volume segmentation by performing several tests for each voxel if it can be deleted without leading to a shortening of the centerline or a destruction of connectivity. The flux driven centerline extraction [10] uses the average outward flux (AOF) of the gradient vector field of a Euclidean distance function from the structure's boundary to detect the centerline points: Skeletal points are characterized by singularities of the gradient vector field. As strong singularities correspond to high magnitude AOF, a threshold on the AOF yields an approximation to the sought skeleton. As a simple thresholding on the AOF however does not guarantee a connected skeleton, the AOF is used to guide the removal of voxels in a topology-preserving thinning.

3. EVALUATION

3.1. Quantitative Evaluation

3.1.1. Generation of synthetic data

Our evaluation relies on 4 data sets with isotropic spatial sampling which will be used to assess the method's precision for isotropic data. They are generated using centerlines from [11]: 2 synthetic and 2 real artery geometries (Fig. 2 (a) - (d)). In addition, one larger centerline will be used to generate 6 data sets with anisotropic spatial sampling to evaluate the effect of the anisotropic sampling of CLSM data (Fig. 2 (e)). We construct synthetic tubular objects of known radius around these centerlines according to the convolved-bar like model. All data sets exhibit a radius of 3 except data set 4 which has a radius of 1 because it has many thin and closely located vessels.

To generate synthetic image data from these objects, we simulate the imaging process in a CLSM which consists of the following aspects: (i) CLSM PSF modeled by an anisotropic 3D Gaussian, (ii) anisotropic spatial sampling of the 3D object and (iii) photon-counting noise modeled by a Poisson distribution. The anisotropic spatial sampling - i.e. the resulting voxel size - chosen for the image acquisition is directly related to the CLSM PSF as the PSF limits the resolution. The CLSM PSF can be modeled by a 3D-Gaussian [12]. The image data we have acquired with our Zeiss confocal microscope (LSM710) exhibit in the worst case voxels of $VoxelSizeXY = 66nm$ in the dimensions of the image plane and $VoxelSizeZ = 396nm$ in the dimension along the optical axis which is a sampling anisotropy of $SA = \frac{VoxelSizeZ}{VoxelSizeXY} = 6$ between the third dimension and the other two dimensions. From the first 4 centerlines, we will generate isotropic data convolved with an isotropic Gaussian (equal

standard deviation in all dimensions: $\sigma_x = \sigma_y = \sigma_z = VoxelSizeXY$) and corrupted by Poisson noise. To assess the influence of the anisotropic spatial resolution on the precision of the segmentation result, using the largest centerline, we generate 6 data sets with varying SA from $SA = 1$ (isotropic spatial sampling) to $SA = 6$. Simultaneously, we change the support of the Gaussian PSF model in the third dimension from isotropic to anisotropic ($\sigma_z = 6 \cdot \sigma_x$) while the standard deviations in the dimensions of the image plane remain constant. Finally, Poisson noise is added to the data.

3.1.2. Evaluation measures

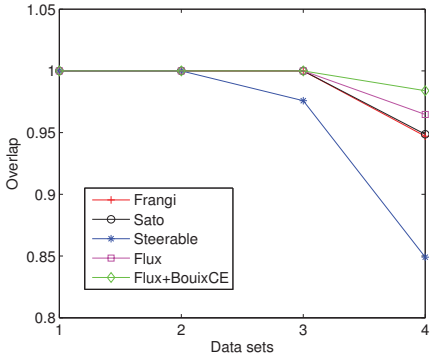
As our goal is to transfer the centerline into a graph representation that characterizes the keratin network, our evaluation criteria are connectivity preservation, extraction capability and extraction accuracy. To assess connectivity, we perform a connected component analysis and compare the number of connected components of reference and computed centerline. For the validation of extraction capability and accuracy, we have to classify all centerline points into three classes: true positive (TP), false negative (FN) and false positive (FP). A point of the reference centerline is considered TP_R if a point can be found on the centerline to be evaluated whose Euclidean distance is smaller than the radius of the line. Otherwise, it is FN. A point of the centerline to be evaluated is labeled as TP_A if there is a point on the reference centerline at a distance smaller than the radius. If not, it is considered FP. In other words, the centerline extraction is considered successful if the distance of the computed centerline to the reference is smaller than the radius. Based on this classification, we assess the extraction capability of the proposed method using the overlap measure OV [13]:

$$OV = \frac{\|TP_R\| + \|TP_A\|}{\|TP_R\| + \|TP_A\| + \|FP\| + \|FN\|} \qquad (1)$$

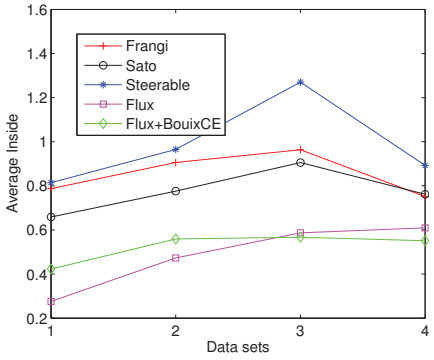
Extraction accuracy can only be assessed where the extraction succeeded. Thus, we use the accuracy measure *Average Inside* (AI) [13] which measures the mean Euclidean distance between reference and automatically computed centerline considering only points that are classified as TP_R.

3.1.3. Results

The connected component analysis revealed that connectivity has been preserved by all methods. Concerning extraction capability and accuracy, we compare the results of a multiscale flux-based line enhancement with results achieved using multiscale line enhancement based on the Hessian of Gaussian [4, 5, 6] in combination with the centerline extraction method from [8]. Fig. 3 illustrates the results on the 4 isotropic data sets. As the OOF-based segmentation is clearly superior to segmentations relying on the other line enhancement filters, we further compare it to results achieved with OOF in combination with the centerline extraction from [10] (Fig. 3 Flux+BouixCE).



(a) Overlap



(b) Mean Euclidean Distance

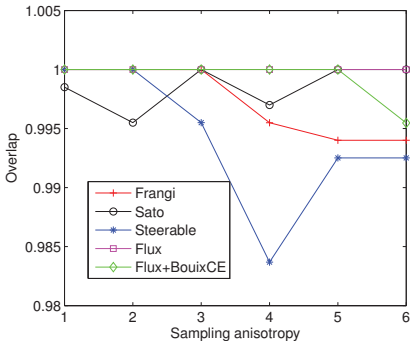
Fig. 3. Evaluation results: (a) Overlap and (b) mean Euclidean distance for each isotropic data set.

The results w.r.t. anisotropic sampling are shown in Fig. 4. The results indicate that again, the flux-based method is superior to the other methods and that the required precision is achieved also for highly anisotropic data. Note that the inconsistency in the AI measure for $SA = 4$ compared to $SA = 5$ or $SA = 6$ of the fifth method (Flux+BouixCE) can be led back to the sensitivity of the centerline extraction method w.r.t. smoothing as discussed below.

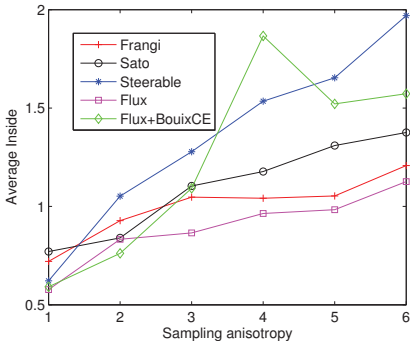
Concerning centerline extraction, we found that the flux driven method's parameter - the AOF threshold - can be set as in [10] for our data, too, making the method virtually parameter-free. However, the method needed a smoothing of the Euclidean distance function before gradient computation in order to perform well with our data. The results were quite sensitive to the amount of smoothing. The results shown in Fig. 3 and Fig. 4 were achieved with a Gaussian smoothing with $\sigma = 1.5$. In contrast, the method from [8] is truly parameter-free.

3.2. Qualitative Evaluation

Fig. 5 shows the performance of the OOF-based line enhancement and centerline extraction from [8] on CLSM image data with a KF network. The connected component analysis reveals that also for KF data the connectivity of the network is being preserved by the proposed method. A visual inspection



(a) Overlap



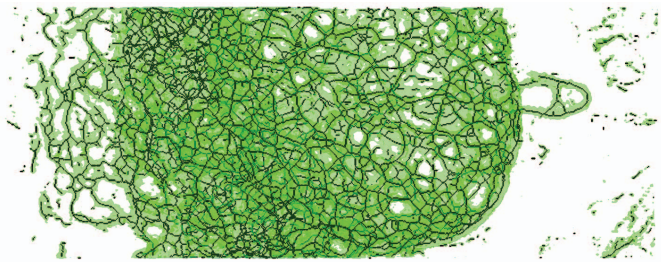
(b) Mean Euclidean Distance

Fig. 4. Evaluation results: (a) Overlap and (b) Mean Euclidean distance for the anisotropic data sets.

leads to the conclusion that the result is virtually artefact-free.

4. CONCLUSIONS

We have presented a flux-based approach towards the 3D segmentation of KFs in CLSM images. To evaluate its accuracy, we have developed synthetic data by simulating the CLSM image formation process. Our quantitative evaluation has shown that the method is subvoxel-precise. Further, a connected component analysis has shown that the network connectivity has been preserved. Taken together, these results are a strong indicator that the network topology can be precisely analyzed by flux-based 3D segmentation.



Segmentation result on KF data as surface representation.

Fig. 5. Segmentation results on KF image: Original image as surface representation (green) and centerlines (black).

5. REFERENCES

[1] S. Kim and P. A. Coulombe, "Intermediate filament scaffolds fulfill mechanical, organizational, and signaling functions in the cytoplasm," *Genes Dev.*, vol. 21, pp. 1581–1597, 2007.

[2] T. Magin, P. Vijayaraj, and R. E. Leube, "Structural and regulatory functions of keratins.," *Exp Cell Res*, vol. 313(10), pp. 2021–32, 2007.

[3] G. Herberich, R. Windoffer, R. E. Leube, and T. Aach, "3d segmentation of keratin intermediate filaments in confocal laser scanning microscopy," in *Proc. 33rd EMBC*. 2011, pp. 7751–7754, IEEE.

[4] F. Aguet, M. Jacob, and M. Unser, "Three-dimensional feature detection using optimal steerable filters," in *Proc. IEEE ICIP 2005*, 2005, vol. 2.

[5] A. F. Frangi, W. J. Niessen, K. L. Vincken, and M. A. Viergever, "Multiscale vessel enhancement filtering," in *MICCAI*, 1998, pp. 130–137.

[6] Y. Sato, S. Nakajima, N. Shiraga, and H. Atsumi et al., "Three-dimensional multi-scale line filter for segmentation and visualization of curvilinear structures in medical images," *MIA*, vol. 2, no. 2, pp. 143 – 168, 1998.

[7] M. W. K. Law and A. C. S. Chung, "Three dimensional curvilinear structure detection using optimally oriented flux.," in *ECCV (4)'08*, 2008, pp. 368–382.

[8] T. C. Lee, R. L. Kashyap, and C. N. Chu, "Building skeleton models via 3-d medial surface axis thinning algorithms," *CVGIP: Graphical Models and Image Processing*, vol. 56, no. 6, pp. 462 – 478, 1994.

[9] H. Homann, "Implementation of a 3d thinning algorithm," *MIDAS Insight Journal*, 2007.

[10] S. Bouix, K. Siddiqi, and A. Tannenbaum, "Flux driven automatic centerline extraction," *MIA*, vol. 9, no. 3, pp. 209 – 221, 2005.

[11] X. Mellado, I. Larrabide, M. Hernandez, and A. Frangi, "Flux driven medial curve extraction," *Insight Journal*, 2010.

[12] B. Zhang, J. Zerubia, and J. Olivo-Marin, "Gaussian approximations of fluorescence microscope point-spread function models," *Applied Optics*, vol. 46(10), pp. 1819–1829, 2007.

[13] M. Schaap, C. T. Metz, T. van Walsum, and A. G. van der Giessen et al., "Standardized evaluation methodology and reference database for evaluating coronary artery centerline extraction algorithms," *MIA*, vol. 13, no. 5, pp. 701 – 714, 2009.